2.1 Properties of strontium titanate

Table 2.1: Summary of the physical properties of $SrTiO_3$.

Property	Value
Lattice parameter at RT (nm)	0.3905
Atomic density (g/cm^3)	5.12
Melting point (°C)	2080
Mohs hardness	6
Dielectric constant (ε_0)	300
Thermal conductivity (W/m.K)	12
Coefficient of thermal expansion (Å/°C)	9.4×10^{-6}
Refractive index	2.31-2.38

2.1.1 Crystal structure

At room temperature, $SrTiO_3$ crystallizes in the ABO_3 cubic perovskite structure (space group *Pm3m*) with a lattice parameter of 0.3905 nm and a density of $r = 5.12\,g/cm^3$. The crystal structure is sketched in figure 2.1. The Ti^{4+} ions are sixfold coordinated by O^{2-} ions, whereas each of the Sr^{2+} ions is surrounded by four TiO_6 octahedra. Therefore, each Sr^{2+} ion is coordinated by 12 O^{2-} ions. Within the TiO_6 octahedra, while a hybridization of the O-*2p* states with the Ti-*3d* states leads to a pronounced covalent bonding [1], Sr^{2+} and O^{2-} ions exhibit ionic bonding character. Hence, $SrTiO_3$ has mixed ionic-covalent bonding properties. This nature of chemical bonding leads to a unique structure, which make it a model electronic material.

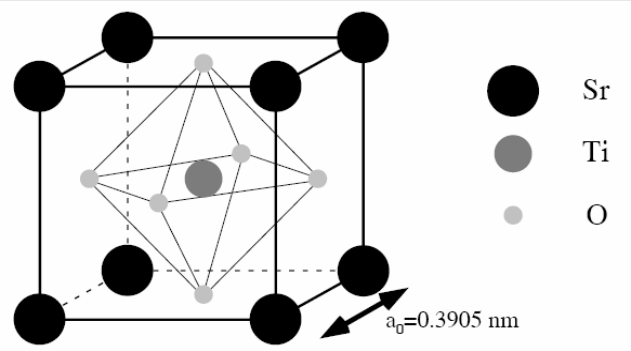

Fig. 2.1 Atomic structure of $SrTiO_3$ at RT. The sizes of the spheres representing the atoms are arbitrary and are not related to atomic radii.

Figure 2.2 shows the atomic arrangements for some of the major (high-symmetry) axial direction in $SrTiO_3$. For any given planar direction (*h*, *k*, *l*) of a perovskite structure, there are always two distinct types of alternating equally spaced atomic planes having different areal densities of the three constituent elements; in this case, Sr, Ti and O. For instance, the (100) $SrTiO_3$ surface can exhibit two different types of atomic alternating planes. One is formed by a TiO_2 plane and the other by a SrO plane [2].

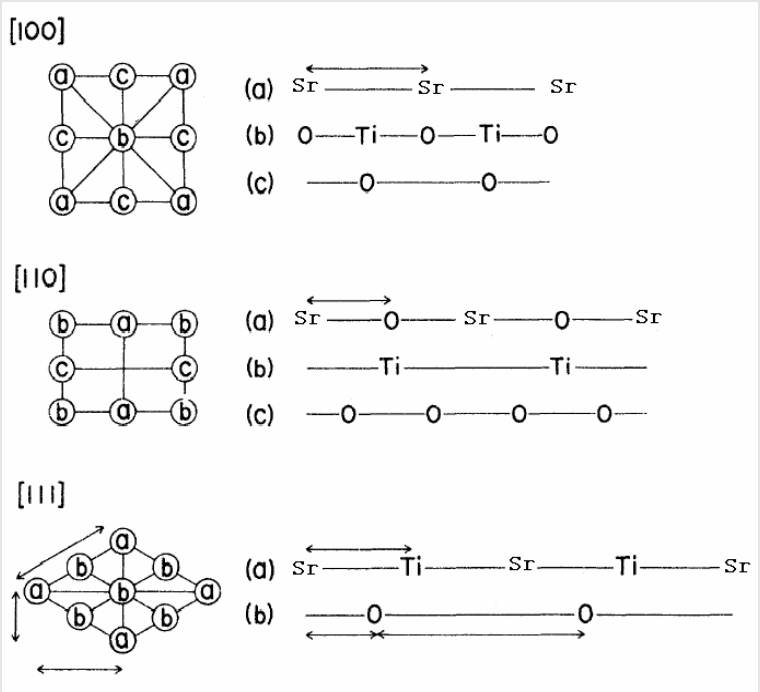

Fig. 2.2 Atomic arrangements for the <100>, <110> and <111> axial directions in $SrTiO_3$. The arrangements shown on the left are end views of the channels, and the letters refer to the individual rows shown on the right.

A distortion from cubic to lower symmetries occurs if the temperature is lowered or if a foreigner cation/dopant is introduced in the lattice (e.g. ion implantation). Distortions are

assigned to three main effects: size effects, deviations from the ideal composition and the Jahn-Teller effect. It is rare to identify a single effect as responsible for distortion of a certain perovskite. As an example of the complexity, cubic $SrTiO_3$ at RT has three more phase transitions upon cooling. $SrTiO_3$ bulk crystals are considered to be; tetragonal ($a = b \neq c$ and $c_{\max} = 0.39\,nm$; space group *I4/mcm*) between 110 K – 65 K, due the opposite rotation of neighbouring oxygen octahedra, orthorhombic in the range 55 K – 35 K and possibly rhombohedral below 10K as X-ray diffraction studies suggest [3], [4]. In fact there is no experimental evidence confirming for sure which structure $SrTiO_3$ exhibits below 10K. Recently, PAC studies on the subject have confirmed that at 10K a single low-symmetry phase is formed, which is not characterized by axial symmetry [5].

Size effects

The degree of crystallographic distortions of most perovskites, accommodating different size cations, can be predicted by the Goldschmidt criterion [6]. Using simple geometry and knowledge of crystal chemistry Goldschmidt defined a tolerance factor *t* of the perovskite-type ABO_3 defined as

$$t \equiv \frac{r_A + r_O}{\sqrt{2}(r_B - r_O)} \tag{2.1}$$

where r_A is the ionic radius of atom A, r_B is the ionic radius of atom B, and r_O is the ionic radius of oxygen. The ideal cubic perovskite $SrTiO_3$ has $t = 1$, $r_A = 1.44$ Å, $r_B = 0.605$ Å, and $r_O = 1.40$ Å. However, if t shows deviation from 1 this might indicate the formation of a perovskite structure of non-ideal type, which is predicted for $0.89 < t < 1$. The factor becomes smaller than 1 if the A ion is smaller than the ideal value or if the B ion is too large. As a result

the BO_6 octahedra will tilt in order to fill space and the symmetry of the crystal structure is lowered. For example $CaTiO_3$ with $t = 0.82$ is orthorhombic.

On the other hand, if *t* is larger than 1 due to a large A or small B ion then tetragonal and hexagonal variants of the perovskite structure are stable, *e.g.* $BaTiO_3$ ($t = 1.062$) and $BaNiO_3$ ($t = 1.13$) type structures. In these cases the close packed layers are stacked in tetragonal and hexagonal manners in contrast to the cubic one formed for $SrTiO_3$. Since perovskites are not truly ionic compounds and since the values are taken for the ionic radii, the tolerance factor is only a rough estimate giving an indication for compounds with a high degree of ionic bonding.

The distortions exhibited by perovskites as a consequence of cation substitution can be used to fine tune and adjust properties of interest. Some of these include conductivity, dielectrics, and colossal magnetoresistance as discussed later in this chapter.

Changing the composition from the ideal ABO_3

Oxygen deficiency

Many ABO_3 perovskites with reducible B-cations can form vacancy-ordered superstructures of general formula $A_nB_nO_{3n-1}$. That is, oxygen deficient perovskites may be formed if the valence of the B-cation can be changed either by heat treatment in oxidizing/reducing atmospheres or via doping in the A-sublattice. The oxygen content varies accordingly and the oxygen vacancies are ordered preferentially with respect to local structure, i.e octahedral, square pyramidal, tetrahedral or square planar coordination. An example is the family of compounds $SrFeO_n$ ($2.5 \le n \le 3$). The valency of the Fe ions can be changed by heating in oxidizing/reducing environment. As a result the oxygen content can vary in between 2.5 and 3. For example in $SrFeO_{2.875}$ some Fe ions can be assigned to the oxidation state +3 and others to +4. The oxygen vacancies order so that FeO_5 square pyramids are formed, see Figure 2.3. The $SrFeO_n$

compounds are examples of defect perovskites, which kept interest in them high, not only for their defect structural chemistry, but also because of two oxidation states of the metallic cation. Furthermore, many oxygen deficient perovskites become good ionic conductors as the number of oxygen vacancies increase in systems like $Sr_n(Fe/Ti)O_{3n-1}$ by replacing Ti for Fe.

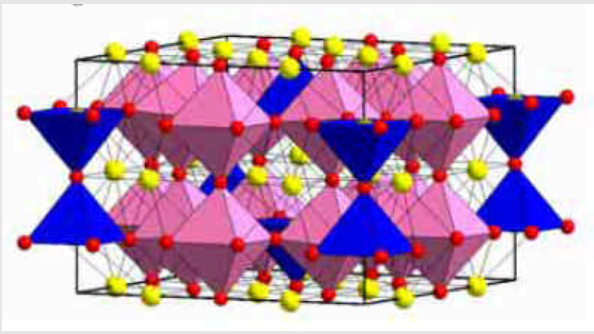

Fig. 2.3 Ordering of oxygen vacancies in $SrFeO_{2.875}$ (=$Sr_8Fe_8O_{23}$). Fe ions are located in both square pyramids and in octahedral.

Cations order

The perovskite structure can also tolerate the presence of more than one cation A and B sites resulting in multiple perovskites such as $AA'B_2O_6$, $A_2BB'O_6$ and $A_3BB'_2O_9$, etc [8][9][10][11]. Ordering of cations at the A and B sites of these perovskite structures is an important phenomenon. For instance, realization of half-metallic ferrimagnetism in Sr_2FeMO_6 ($M = Mo$, Re) depends crucially on the ordering of the B site cations in the perovskite structure.

Jahn-Teller effects

Besides the variations of the perovskite structure due to the effects referred above, there are other distortions of the perovskite structure namely, ferroelectric distortion due to the second order Jahn-Teller effect (SOJT) of the d^0 cations at the B-site (e. g. $SrTiO_3$) and distortions due to core polarization of s^2 cations (eg. Pb^{2+}, Bi^{3+}) at the A site. Also a first order Jahn-Teller (FOJT) distortion (due to unsymmetrical filling of d electrons in t_{2g} and e_g orbital of B cation)

in individual BO_6 octahedra, which could operate in a cooperative manner, can give rise to distorted structures (e. g. $LaMnO_3$).

2.1.2 Electronic structure

The diverse materials properties of ABO_3 perovskite oxides in general, and $SrTiO_3$ in particular, could be traced to their crystal and electronic structures. While a rigorous understanding of the structure vs. property relations would involve extensive electronic structure calculations based on density functional theory [11], a qualitative understanding is possible on the basis of chemical bonding considerations. Many of the $SrTiO_3$ properties can be understood in terms of the electronic structure of the d^0 TiO_6 octahedron in its undistorted form. That is, the Ti cation is in the centre of the octahedron creating equal Ti-O bonds.

Bonding within BO_6

In its stoichiometric form ($Sr/Ti = 1, O/Sr = 3$), $SrTiO_3$ is a good insulator with a 3.2 eV band gap (at T=0K), separating the valence bands from the conduction bands [12]. Due to the sixfold coordination of Ti ions by surrounding O ions, a crystal field splitting of the degenerated Ti-*3d* states of 2.4eV appears. These separated states are called Ti-*3d* t_{2g} and Ti-*3d* e_g. Figure 2.4 shows the schematic electronic structure for a typical undistorted TiO_6 octahedron where the Ti cation has d^0 electronic configuration. In the band picture, the valence band that corresponds to the highest occupied molecular orbitals (HOMO) is mainly atomic (oxygen *2s* and *2p*), and the conduction band, which corresponds to the lowest unoccupied molecular orbitals (LUMO) is mainly cationic, arising from the empty *d* states. The gap between the HOMO and the LUMO states makes $SrTiO_3$ a band insulator. The Sr site cations in $SrTiO_3$ are in general strongly electropositive and hence they play a secondary role in the electronic structure. Often, their size

plays a crucial role in modifying the TiO_6 connectivity of the $SrTiO_3$ structure and hence the electronic structure.

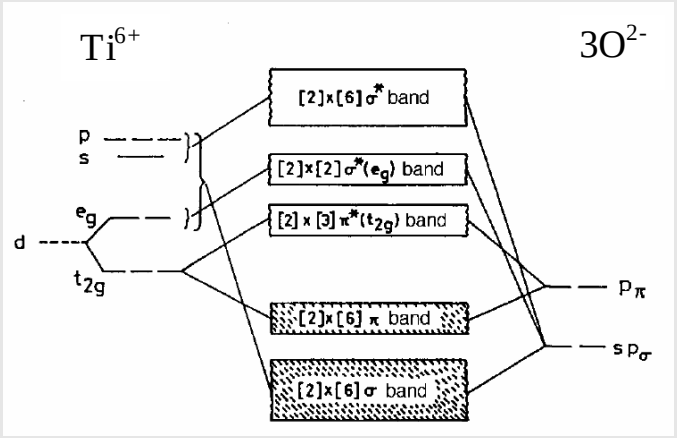

Fig. 2.4 Schematic electronic structures for TiO_6 octahedron of a typical $SrTiO_3$ oxide with d_0 electronic configuration for the Ti ion, from.

The presence of intrinsic defects, such as vacancies, and the appearance of extrinsic defects like dopants lead to modifications of the electronic structure and the electronic conductivity of the material. Thereby, a defect model to account for the observed variations in electrical conductivity on both undoped and doped $SrTiO_3$ material was purposed in 1995 by M. Javed Akhtar et al. [13]. The calculations show that in $SrTiO_3$ intrinsic defects are O and Sr vacancies, whereas Ti vacancies are of minor importance due to the high value of the energy of formation.

The addition of acceptor dopants into the $SrTiO_3$ lattice creates a defect with an effective negative charge relative to the host lattice. The electroneutrality can be compensated by either oxygen vacancies doubly ionized, $V_{\ddot{O}}$, electron holes, h, or donor impurities. In the n-type regime, the enhancement of the oxygen vacancy concentration by the acceptor impurities will result in a decrease in the conductivity. However, p-type conductivity may arise from the incorporation of oxygen into the impurity induced oxygen vacancies. The onset of the p-type conduction depends on the amount of acceptor impurity added to the sample.

In contrast, donor dopants have an effective positive charge which can be compensated in two ways: (1) by the formation of conduction electrons, the concentration of which will be equal to the concentration of the excessive positive charge, and (2) by the formation of metal vacancies (V''_{Sr}).

Typical examples of acceptor- and donor- doped $SrTiO_3$ are provided by Nb^{5+} (or e.g. Sb^{5+}) and Sc^{3+} (or e.g. La^{3+}), which substitute at Ti^{4+}- and Sr^{2+}- sites, respectively. Cations can substitute into the perovskite lattice with charge compensation in a number of ways. In order to ascertain the feasibility of dissolving the dopant metal oxide into the host lattice, Athkar et al. calculated the solution energy, providing defect formation and lattice energies. According to dopant substitution energies it is possible to predict cattion lattice site location in $SrTiO_3$ based on the combination of ion oxidation state and ionic radius. Table 2.2 summarizes the main conclusions taken from such computer simulations studies performed in $SrTiO_3$. Their reliability may be experimentally studied by the EC technique and moreover, the fraction of dopant atoms at several substitutional and interstitial sites may be determined by EC studies. Chapter 5 brings this topic to discussion.

Table 2.2: Most energetically favourable impurity cation substitution into $SrTiO_3$ according Akhtar model.

Impurity oxidation state	Lattice sites predominantly substituted by impurity ions: Sr^{2+}	Ti^{4+}	Most probable charge compensation mechanism	Impurity incorporation in Sr- and/or Ti- sites is enhanced for:
+1	×		Oxygen vacancy compensation	$R_i \sim 0.9$ Å
+2	×		No charge compensation is required	$R_i \sim 1.05$ Å
	×		Electron compensation	$R_i > 0.94$ Å
+3		×	Oxygen vacancy	$R_i < 0.94$ Å
	×	×	Self-compensation	0.89 Å $< R_i < 0.94$ Å
+4		×	No charge compensation is required	$R_i < \sim 0.76$ Å
	×		Electron compensation	$R_i > \sim 0.76$ Å

2.1.2.1 Electronical and magnetic properties

The TiO_6 octahedra in $SrTiO_3$ form a metallic three dimensional network, so that, electric conduction is three-dimensional along the TiO_6 network, which is stable for substitutions of the Sr-site ion. That is, the Sr site cation is completely ionized in most cases without contributing to the band formation. By this ionization of the Sr-site, electrons are left in the oxygen *2p* bands and/or the Ti d^0 bands. For d^n $(n > 0)$ configuration, the number of electrons left on those bands may be modulated by the presence of other TM cations, which alters $SrTiO_3$ properties. While magnetism and electronic properties are usually related to unfilled *3d* electron shells of TM ions incorporated on the B site [14], pronounced dielectric properties are connected with filled *3d* electron shells. Electronic correlations [15] of such *3d* states are generally strong, as the buckling of the $TM - O - TM$ angle reduces the band width, W, as a consequence of changing the ionic radius of the Sr-site ion. This increases the ratio of the Coulomb interaction, U, relative to W, since the effective *d*-electron transfer interaction between the neighbouring B sites is governed by the supertransfer process via the O *2p* state. Thereby, the properties and phase diagrams of a perovskite strongly depend on non-stoichiometry and even more on tilting or distortions of the BO_6 octahedra. Further aspects rely on order/disorder processes of the orbital part of the *3d* wave function, charge doping and charge/orbital inhomogeneous states that lead to colossal response, *e.g.*, to external magnetic fields [16].

Before, however, such effects become relevant, the physical properties of the system are given by a hierarchy of energies based on the electronic structure, *i.e.*, the number of *3d* electrons, the Hunds Rule coupling, the crystalline electric field or Jahn-Teller splitting of the *3d* electron states and finally due to exchange energies.

2.1.2.2 Optical properties of the *d*-band $SrTiO_3$

The relation between the electronic structure of the solid and its optical properties such as reflectivity or absorption are established through the optical dielectric function. Since it is susceptible to vary with temperature, optical constants (e.g. reflective index) are also expected to vary. For instance, the isotropic optical properties of insulating $SrTiO_3$ perovskite in the visible and ultraviolet regions are drastically changed by cooling the crystal down to liquid helium temperature. The dielectric constant and refractive index increase by a factor of 10 and 10^2, respectively.

In addition to thermal activation, reducing or doping $SrTiO_3$ can confer it semiconducting or superconducting (if T ~ 0.7 K) properties. The reason is related with the broadening of the energy levels of the titanate octahedron and to the coexistence of free and delocalized (self-trapped) excitations.

Due to the separation of absorption and emission processes, energy transfers are of crucial importance for optically doped semiconductors. These are best facilitated by formation of intermediate stages bridging the highly localized states of the doping ion with extended orbitals of the matrix, which results in small activation energies. Nevertheless, emission efficiency is sensitive to thermal quenching variations and this hinders their practical applications in the solid state light emitting devices.

Finally, light interaction with the electrons of a solid through the electromagnetic field, associated with the light wave, can be used to obtain unique information on optically doped semiconductors. For instance, $SrTiO_3$ optimal annealing temperature, up to which occurs optical activation, following ion implantation may be determined by means of PL spectroscopy. Indeed this has been investigated by Karl Johnston and Ulrich Wahl in a ^{89}Sr-implanted $SrTiO_3$ sample

of this work. They found that a mean band edge luminescence reappeared only after annealing at 800 ºC, which further improved upon annealing at 1000 ºC. Several broad emission bands in the visible region have been observed; most prominently a green emission band centred around 2.4 eV or 250 nm. The sharp emission lines may be due to crystal defects resulting from implantation process, e.g. Sr interstials or, to impurities which were already present in the as grown sample. The referred investigation is still in progress.

2.1.3 Synthesis

The commercially available $SrTiO_3$ single crystal samples utilized in this work have been grown by the Verneuil or flame fusion method, cut and polished on a <100> surface [17]. It is a rapid process, capable of controlling to some extent the structural perfection of the growing crystal and providing large crystals. The principle of the process involves melting a thinly powdered substance using an oxyhydrogen flame and crystallizing the melted droplets into a boule. By means of a custom-oriented seed crystal it is possible to achieve a specific desired crystallographic orientation of growth. The process was developed in 1902 by the French chemist Auguste Verneuil who achieved for the first time control of nucleation and thus single crystals, of ruby and sapphire with melting points above 2000ºC, see a process simplified block diagram figure 2.5. Verneuil also extended the process to the production of other stones like diamond, rutile and strontium titanate ($SrTiO_3$). The Verneuil process is considered to be the founding step of modern industrial crystal growth technology and remains virtually unchanged of a wide use to this day. In fact, the principles of the method with nucleation grow rate and diameter control have been applied in most of the growth processes described in the following years. An example is the Czochralski process, which has found numerous applications in the semiconductor industry, where a much higher quality of crystals is required than the Verneuil process can produce.

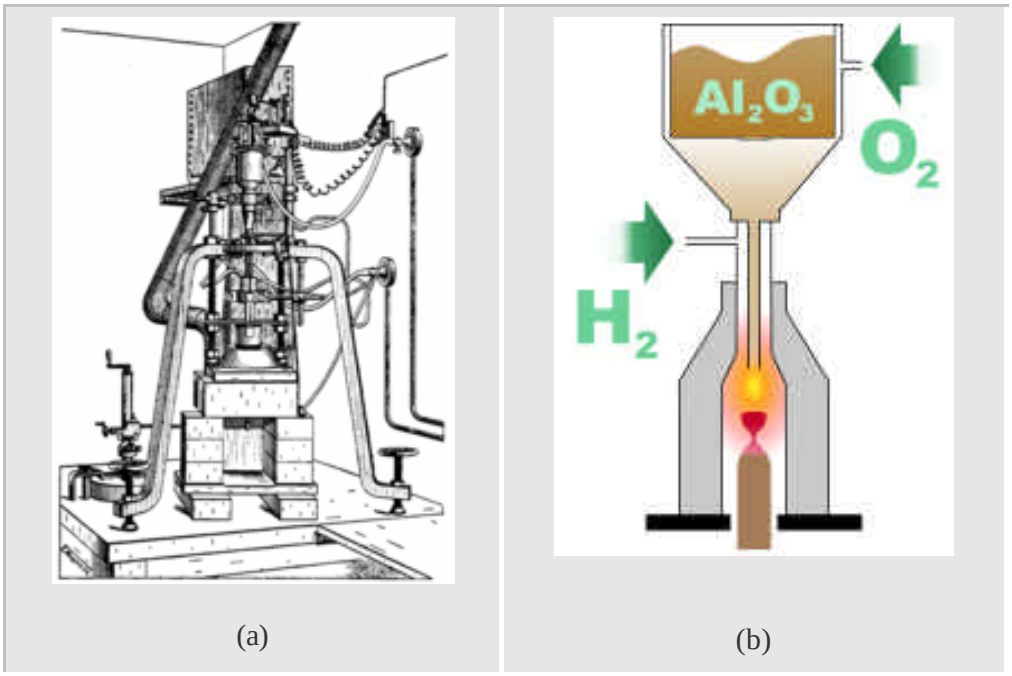

Fig. 2.5 (a) Picture of an early furnace used by Verneuil to synthesize rubies using the Verneuil process schematized in (b).

2.2 Ion implantation as a doping technique in $SrTiO_3$

Ion implantation was first applied to semiconductors over 40 years ago as means of introducing controllable concentrations of n- and p-type dopants at precise depth below the surface. It is now an indispensable process in the manufacture of integrated circuits. However, because other doping methods (e.g. diffusion during crystal growth) have been widely used, ion implantation of perovskite oxides is still in its infancy. A great deal has still to be learned about the production and processing of perovskite oxides (including thin films) suitable for: (1) high temperature semiconducting (HTS) electronic devices, (2) solid oxide fuel cell (SOFC) applications and colossal magnetoresistance (CMR) thin film devices for recording [18][20]. In this context, ion implantation gained a renewed interest as means to alter the near-surface optical, electrical, or mechanical properties of ceramic materials such as $SrTiO_3$. For many of the potential applications, it will be necessary to anneal these materials following implantation

in order to remove the damage associated with the implantation process. In this context, optimal annealing temperature of $SrTiO_3$ has been investigated and will be later discussed. The following sections focus on the preparation and influence of several implanted impurities lattice sites on the optical, electrical and magnetic properties of $SrTiO_3$, providing thus additional insight into the relevant applications of impurities in $SrTiO_3$ referred above.

2.2.1 Electrical doping

The purpose of dopant implantation is to introduce electrically active n- or p-type dopants to increase the free carrier concentration, while the aim of implantation isolation is to produce highly resistive layers by implantation of various elements, which create mid-gap levels that trap electrons and holes.

In the case of $SrTiO_3$ the most important criterion for a possible substitution of Sr- or Ti-site ions by dopants is a comparable ionic radius of the corresponding species. Dopants with a higher (lower) oxidation level than the host ion act as donors (acceptors). However, group III dopants constitute an exception to this rule since they are amphoteric and can substitute at either Sr-site or Ti-site. When these dopants are lighter or of neighbouring masses to the host elements or at low concentration, then ion beam techniques are not able to determine the implant site, when the "emission channeling radioactive nuclear technique" shall be used. In the following some examples for each type of dopant are given.

Possible donors: Trivalent ions such as Al^{3+}, La^{3+} ions on Sr^{2+} sites or pentavalent ions such as Nb^{5+}, Ta^{5+} ions on Ti^{4+} sites act as single donors.

Possible acceptors: Fe^{3+} as trivalent ions on Ti^{4+} sites, or Na^{1+} as monovalent dopant on Sr^{2+} sites, may act as single acceptors.

Amphoteric: Group *Ib* elements can act as donors or acceptors depending on for which cation they predominantly substitute (e.g. Cu and Ag).

Consequently, the incorporation of donor and acceptor dopants into the lattice lead respectively to an excess of positively charged carriers or to an excess of negatively charged carriers in the perovskite lattice. This is due to the fact that the electronic states introduced within the crystal band gap by donor and acceptor impurities are either located near the valence or conduction bands thermally absorbing or injecting electrons into the material, and thus, leading to p- or n-type material, respectively. Finally since the thermal energy of the electrons at RT is ~25 meV, the energy difference between the introduced level and the valence or conduction band should be of the same order of magnitude to have efficient ionization of the dopants.

The precise position of these levels within the band gap depends on the chemical properties of the impurity, on its lattice site within the crystal and on possible interactions with other defects and impurities. An impurity element at interstitial sites will introduce different levels than when placed at substitutional sites.

Despite of all the studies performed in doped $SrTiO_3$, the rich variations in physical properties arising from carrier doping are not yet thoroughly understood. While n-type conductivity, achieved by substituting Nb^{5+} (or La^{3+}) for Ti^{4+} (or Sr^{2+}) has been found and gave rise to practical applications (e.g. electrodes and gas sensors), p-type conductivity in $SrTiO_3$ is not confirmed. In fact, the investigation on p-type doped $SrTiO_3$ is little, made both experimentally and theoretically. Higuchi et. al experimentally have reported the electronic structure of a p-type $SrTiO_3$ single crystal in which the acceptor ion Sc^{3+} is introduced into the Ti^{4+} site [21], while the effect of Sc^{3+} on the electronic properties has been studied by Weidong Lue et al using *ab initio* pseudo-potential density functional theory [22]. Moreover, Shouyu Dai et al have found that $SrTiO_3$ exhibits p-type conductivity when doped by the substitution of In for Ti [23]. Theoretical investigation of In doped $SrTiO_3$ performed by Zhang Zhi-Yong

revealed that the electronic structure and optical properties of the system display p-type semiconductor features [24]. So, further experimental investigation is required.

The difficulty in obtaining p-type conductivity in donor doped $SrTiO_3$ might be connected with its stronger tendency to develop Sr-rich microcrystals on the surface during heat treatment under oxygen atmosphere compared with undoped or acceptor-doped crystals, respectively [25].

2.2.2 Magnetic doping

RT ferromagnetism is being actively investigated in several semiconducting oxides such as $SrTiO_3$ and $BaTiO_3$, namely when doped with Mn or Co by direct ion implantation [26]. The origin of the ferromagnetism, however, is in all these cases poorly understood. One of the key unanswered questions is whether the materials indeed contain uniformly distributed transition-metal or rare earth (RE) impurity elements or contrarily, these are distributed as clusters, precipitates or second microscopic phases that are responsible for the observed magnetic properties. Most studies reported in the literature have produced dilute magnetic semiconductors either by introducing the dopant during bulk crystal growth or by one of the following techniques: molecular beam epitaxy (MBE), metal-organic chemical vapour deposition (MOCVD) of single crystalline layers, sputter deposition or pulsed laser deposition (PLD) of thin polycrystalline layers [27]. Despite the fact that, so far ion implantation has been little used, it might present advantages, since it is less likely to suffer from the formation of second phases and hence may be superior with respect to the realization of single-crystalline magnetic nanolayers. Moreover, as a matter of fact there are also strong indications that the defects which are specifically introduced by ion implantation might even play a crucial role in order to achieve the ferromagnetism. In this context, efforts for producing thin nanolayers of ferromagnetic semiconductors by means of ion implantation are being undertaken. The origin of

the magnetism in semiconductors has been investigated by a combination of structural, magnetic, optical and transport characterization techniques [28].

Semiconductors showing ferromagnetism at RT will be very promising materials since they would be a key issue for the realization of future spintronic devices like spin-transistors, non-volatile semiconductor memory, or polarized optical emitters. These devices aim not only to make use of the charge of electrons, but also of their spin state.

For these reasons, a first attempt to investigate the possibility of producing diluted magnetic semiconductors by means of ion implantation was performed in the $SrTiO_3$ semiconducting oxide by implanting Fe to different doses. The created nanolayers were investigated by combining RBS/C and PIXE/C structural characterization techniques, electron emission channeling nuclear technique and finally, magnetic characterization with a superconducting quantum interface device (SQUID). This work is presented and thoroughly discussed in chapter 5.

2.2.3 Optical doping

Similar to electrical doping, the term optical doping is used to describe the incorporation of impurities, in particular RE and transition metal (TM) ions, in a host material to enhance and/or tailor its optical properties. A distinction has to be made between optical dopants used to tailor emission and absorption. In optoelectronics technology, i.e., which forms the basis for components such as semiconductor lasers, optical discs, image sensors or optical fibres, attractive systems are formed by combining atomic-like properties of dopants with band structure of the host material. In particular, narrow emission lines with temperature independent wavelengths due to transitions with the $4f$ electron core of the RE ion can be activated by efficient band-to-band absorption of the matrix, or by carrier injection. This makes RE-doped

semiconductors interesting for applications. In particular, after discovering that $SrTiO_3$ may be a blue light emitter, new perspectives for the realization of $SrTiO_3$ based optoelectronic devices, operating in the GHz regime, started emerging. Different methods are being explored, either based on electron doping, i.e., by Nb doping or through an annealing process suitable for producing oxygen vacancies [29], or by Sr substitution with Nb and La [30] or Ar^+ ion irradiation [31]. The mechanism of this blue luminescence is different from that of the well known greenish emission of stoichiometric $SrTiO_3$ at low temperature [32]. In addition, a large body of work on the optical properties of metal ions with a partially field *d*-shell containing perovskites exists. Cr^{3+} ions with d^3 configuration have been used to investigate the optical properties of $SrTiO_3$. The TM metal doped titanates became of interest after the discovery of photoelectrochemical water splitting by titanates [33]. It appeared possible to sensitize an $SrTiO_3$ electrode for visible light by doping with transition metal ions [34]. The optical transitions involved were shown to be of the metal-to-metal charge transfer type, e.g., $Cr^{3+} + Ti^{4+} \rightarrow Cr^{4+} + Ti^{3+}$, which are responsible for the brownish colour of the composition. In this work, the incorporation of RE and TM in regular lattice sites was investigated by means of the EC technique, which allows to optimize thermal annealing conditions. The Yb-, Ag-, Cd- and Fe-implanted systems will be discussed in chapter 5.

2.3 Applications

$SrTiO_3$ in the perovskite structure is a very attractive material for application to microelectronics because of its high charge storage capacity, good insulating properties and excellent optical transparency in the visible region and chemical stability[35][36][37]. In the past, due to lattice parameter match, $SrTiO_3$ was largely employed as substrate for epitaxial growth of high temperature superconducting films [38].Currently, investigations aim to tune

dielectric properties in $SrTiO_3$ and subsequently optical properties as well. Its high dielectric permittivity at RT (~300) increases even more on cooling and closely follows the Curie-Weiss law between 100K and 240K. This allied to the low microwave losses of $SrTiO_3$, turn it in the most attractive material for tuneable microwave electronics devices such as: phase shifters, filters, delay lines, tuneable oscillators, etc. At temperatures as low as 1K, $SrTiO_3$ may exhibit superconductivity when doped e.g. with Nb, La, Ta or oxygen vacancies. Superconductivity dependency with T_C and subsequently with dopant concentration dependent of the relative concentration of defects; either generated during crystal growth or during the doping process.

$SrTiO_3$ has also attracted a great deal of interest in the world of oxide electronics, not only as a high dielectric constant insulator, but also as a wide-gap semiconductor with a band gap of ~3.2 eV. However, by processing the material in an oxygen reducing atmosphere or by cation substitution at fairly low carrier density (~10^{18} cm^{-3}) it can be made semiconducting. The magnitude of the conductivity and the type of the majority carriers depends on the relative concentrations of defects. Reduction creates oxygen vacancies that act as effective donors. The resulting n-type material can be modified by changing the oxygen partial pressure or by acceptor/donor doping. Conductivity is more accurately controlled by doping than oxygen deficiency control. The ability to control conductivity in $SrTiO_3$ is important in the design of various electroceramic devices such as capacitors, metal oxide semiconductor filled effect transistors (MOSFET's), thermistors and varistors [39]. In the case of MOSFET's manufacture, $SrTiO_3$ is becoming one of the preferred high-K dielectric candidates to replace SiO_2 as the gate insulator when its thickness has to be driven to dimensions as low as the atomic level [40]. Thus, the SiO_2 power consumption increase due to gate current leakage is overcome. $SrTiO_3$ is also preferred in the MOSFET gate manufacture because of its high degree of mismatch with Si

(~1.7%) turning possible the gate production by molecular beam epitiaxy (MBES). The functionality of other metal-insulator-semiconductor (MIS) heterostructures (where $SrTiO_3$ serves as semiconductor) maybe optimized by the deposition method choice. High quality $SrTiO_3$ films on $SrTiO_3$-buffered Si(001) have been deposited by rapid thermal annealing, reactive pulse laser ablation (RPLD) and sol-gel method. The films acts as buffer layers e.g. into optical devices such as waveguides: in this case, the attenuation and propagation coefficients of the wave in the waveguide are likely to be strongly influenced by the film microstructural properties and by the etching quality.

For opening novel applications to electronics, it is necessary to fabricate both n-type and p-type $SrTiO_3$. However, p-type $SrTiO_3$ production is so far little known and is hardly produced because of the compensation effect mainly caused by oxygen vacancies [41]. Nevertheless, p-type $SrTiO_3$ will be a very promising material. First, it would become a wide-gap semiconductor diode in blue-light region and would be highly valued in the semiconductor industry. Second, it is well known that p-type doping perovskite structures accommodate protonic conductivity. The protonic conductors are important materials for a wide variety of electrochemical applications such as fuel cell and hydrogen sensor in the renewable energy-source industry.

Further possible technological applications of titanate-based perovskites, and in particular of $SrTiO_3$, consist in their use as ceramic host phases for the immobilization of actinide and fission-product wastes. Actinide elements produces high-energy alpha particles and low-energy heavy recoil nuclei (alpha recoils) [42], requiring the actinide waste to be incorporated in suitable matrices.

References

[1] R. D. LEAPMAN, L. A. GRUNES, AND P. L. FEJES, *Phys. Rev. B 26*, 614 - 635 (1982)

[2] F.M.F. DE GROOT, M. GRIONI, J.C. FUGGLE, J. GHIJSEN, G.A. SAWATZKY AND H.PETERSEN, *Phys. Rev. B 40* (1989), pp. 5715–5723.

[3] BEHNAZ RAHMATI KALKHORAN, Microstructural Studies on the Reoxidation Behavior of Nb-doped $SrTiO_3$ Ceramics, Max-Planck-Institut für Metallforschung Stuttgart, 2004.

[4] FARREL W. LYTLE, *Journal of applied physics* 35 (1964) 2212.

[5] LIXIN CAO, E. SOZONTOV, AND J. ZEGENHAGEN, *Phys. stat. sol*. (a) 181 (2000) 387.

[6] GOLDSCHMIDT, *Geochemistry*, Oxford University press, 1958.

[7] A.C. MARQUES, J.G. CORREIA, U. WAHL, J.C. SOARES, *Nucl. Instrum. and Methods in Physics Research B* 261 (2007) 604–607

[8] J. B. GOODENOUGH AND J. M LONGO, LANDOLT-BDRNSTEIN, Numerical data and Functional Relationships in Science and Technology; New Series, Group Ill, Ed. K. H. Hellwege, Springer - Verlag, Berlin, Vol. 4a (1970).

[9] J. B GOODENOUGH AND J. A. KAFALAS, *J. Solid State Chem.* , 6, 493 (1973).

[10] J. RODRIGUEZ-CARVAJAL, M. HENNION, F. MOUSSA, A. H. MOUDDEN, L. PINSARD AND A. REVCOLEVSCHI, *Phys. Rev. B*, 57, R3189 (1998).

[11] F. S. GALASSO, Perovskites and High Tc Superconductors, Gordon and Breach, New York (1990); p3 - 51.

[12] N. H. HILL, *Annu. Rev. Mater. Sci.*, 32, 1-37 (2002).

[13] M. JAVED AKHTAR, ZEB-UN-NISA AKHTAR, AND ROBERT A. JAKSON, *J.Am. Ceram. Soc.*, 78 [2] 421-28 (1995).

[14] M. CARDONA, *Phys. Rev. 140*, A651 (1965).

[15] R. WASER, T. BAIATU, AND K.-H. HÄRTL, *J. Am. Ceram. Soc.* 73, 1645 (1990).

[16] P. A. COX, Transition Metal Oxides (Clarendon Press, Oxford,1995).

[17] P. LEMMENS AND P. MILLET, Spin - Orbit - Topology, a Triptych, *Lect. Notes Phys.* 645, 433–477(2004)

[18] M. CARDONA, PHYS. REV

[19] Y. TOKURA, *Physics Today* 56, 50, July (2003)

[20] M.CAPIZZI AND A. FROVA, *Phys. Rev. Lett*. 25, 1298 (1970).

[21] K. W. BLAZEY, *Phys. Rev. Lett.* 27, 146 (1971).

[22] E. SCHENEIDER, P. J. CRESSMAN, AND R. L. HOLMAN, *J. Appl. Phys.* 53, 4054 (1982).

[23] T. TOYOTA AND M.YABE, *J. Phys. D: Appl. Phys*. 16, L251 (1983).

[24] S. BARKER AND M. THINKAM, *Phys. Rev.* 125,1527(1962).

[25] J. L. SERVOIN, Y.LUSPIN AND F. GERVAIS, *Phys. Rev. B* 22, 5501 (1980).

[26] W. S. BAER, *Phys. Rev.*144, 734, (1966).

[27] F. F. SCHOOLEY, W. R. HOSLER, AND M. L. COHEN, *Phys. Rev. Letters* 12, 474 (1964).

[28] L. G. J. DE HAART, A. J. DE VRIES AND G. BLASSE, *J. Solid State Chem*, 59-4 (1985) 291-300.

[29] L. G. TEJUCA, J. L. G. FIERRO, Properties and Applications of Perovskite-type Oxides, Edited by CRC Press, 1992.

[30] T. MONTEIRO, M. J. SOARES, C. BOEMARE, E. ALVES, J.G CORREIA, *Rad. Eff. Def. Solids* 157 (2002) 1071-1076.

[31] L. GRABNER, *Phys. Rev.* 177 (1969) 1315-1323.

[32] R. LEONELLI, J.L. BREBNER, *Phys. Rev. B* 33 (1986) 8649-8656.

[33] THOMAS WOLFRAM, SINASI ELLIALTIOGLU, Electronic and Optical Properties of d-Band Perovskites, Cambridge University Press, 2006.

[34] Commercially available from *CrysTec GmbH*, 12555 Berlin, Germany.

[35] T. KOLODIAZHNYI, A. PETRIC, *J. of Electroceramics*, Volume 15, Number 1, September 2005 , pp. 5-11(7).

[36] L. E. REHN, *Nucl. Instrum. and Methods*, B64, 161 (1992).

[37] P. RAMIREZ, COLOSSAL MAGNETORESISTANCE, J. Phys.: Condens. Matter 9 (1997) 8171-8199.

[38] T. HIGUCHI, T. TSUKAMOTO, N. SATA, M. ISHIGAME, Y. TEZUKA AND S. SHIN, Phys. Rev. B 57 (1998) 6978.

[39] W. D. LUO, W. H. DUAN, S. G. LOUIE AND M. L. COHEN, Phys. Rev. B 70 (2004) 214109.

[40] Y. S. DAI, H. B. LU, F. CHEN, Z. H CHEN, Z. Y. REN AND D. H. L. NG, Appl. Phys. Lett. 80 (2002) 3545.

[41] ZHANG ZHI-YONG *et al*, Chinese Phys. **16** (2007) 2791-2797.

[42] A. GUNHOLD, L. BEUERMANN, M. FRERICHS, SURFACE SCIENCE, 523 (2003) 80.